Supporting Information

Synergistic Cs/P Co-doping in Tubular g-C_3N_4 for Enhanced Photocatalytic Hydrogen Evolution

Juanfeng Gao, Xiao Lin *, Bowen Jiang, Haiyan Zhang and Youji Li *

National Experimental Teaching Demonstration Center for Chemistry, College of Chemistry and Chemical Engineering, Jishou University, Jishou 416000, China

2.1 Synthesis of P-Doped Tubular Carbon Nitride

2.1.1 Synthesis of different concentrations P-Doped Tubular Carbon Nitride

Phosphorus-doped tubular carbon nitride was synthesized through a two-step process involving hydrothermal treatment followed by calcination, with melamine and phosphorus acid (H_3PO_4) as the starting materials. Briefly, a specific amount of melamine was dispersed in a 2 mol/L H_3PO_4 (8 mL) solution and stirred in a water bath at 60°C for 0.5 h. The resulting solution was then transferred into a Teflon-lined stainless steel autoclave and heated at 180°C for 10 h. After cooling to room temperature, the precipitate was collected, washed several times with deionized water, and dried at 60°C for 12 h, yielding the precursor material for tubular carbon nitride, denoted as Pre-PTCN. Finally, the Pre-PTCN was placed in a covered crucible and heated to 500°C at a rate of 2.5°C min^{-1} under an N_2 atmosphere, followed by maintaining the temperature for 4 h. The product was then naturally cooled to room temperature, yielding phosphorus-doped tubular g-C_3N_4, designated as P-TCN. To systematically study the relationship between doping concentration and performance, a series of PTCN-x catalysts (x = 6, 10, 12, 14) were synthesized by varying the amount of H_3PO_4 (6 mL, 10 mL, 12 mL, 14 mL) while maintaining the same heat treatment parameters.

2.3 Material Characterizations and Photocatalytic (Photoelectrochemical) Tests

2.3.1 Material Characterizations

The surface morphology of the photocatalysts was examined using scanning electron microscopy (SEM, ZEISS SIGMA-500) and transmission electron microscopy (TEM, JEOL JEM-2100), acceleration voltage of 200 kV. Elemental composition was analyzed by energy-dispersive X-ray spectroscopy (EDX, JED-2300T) at an accelerating voltage of 200 kV. Fourier-transform infrared spectroscopy (FTIR, Nicolet IS10) was employed to identify surface functional groups, and the crystal structure was determined by X-ray diffraction (XRD, Bruker D8). The chemical states of the elements were characterized using X-ray photoelectron spectroscopy (XPS, Thermo Fisher ESCALAB 250xi), 284.8 eV was used as an exogenous carbon correction peak. UV-visible diffuse reflectance spectra (DRS, Shimadzu UV-2600) were recorded with

$BaSO_4$ as the reference material. Photoluminescence (PL) emission spectra were obtained using a fluorescence spectrophotometer (Jasco FP-8300).

2.3.2 Photoelectrochemical Measurement

Photoelectrochemical measurements were conducted using a standard three-electrode system on a CHI 650E electrochemical workstation, with 0.1 M sodium sulfate solution serving as the electrolyte. The working electrode was prepared by dispersing the photocatalyst (10.0 mg) in a mixture of ethanol (1.00 mL) and Nafion (20 μL), followed by 30 minutes of ultrasonication. The resulting dispersion was uniformly coated onto fluorine-doped tin oxide (FTO) glass and dried in an oven at 60 °C. A platinum wire and an Ag/AgCl electrode were used as the counter and reference electrodes, respectively. Photocurrent measurements were performed under visible light irradiation for 300 seconds using a 300 W xenon lamp. Electrochemical impedance spectroscopy (EIS) was conducted within a frequency range of 0.01 Hz to 100 kHz under the same three-electrode setup. The open circuit voltage was used as the reference for parameterization. Mott-Schottky plots were recorded at an AC voltage amplitude of 5 mV with frequencies of 500 and 1000 Hz.

2.3.3 Photocatalytic Hydrogen Experiments

Typically, 20 mg of catalyst was dispersed in 50 mL of an aqueous methanol solution (CH_3OH, 20 vol%), with 1% K_2PtCl_6 added as a co-catalyst deposited onto the catalytic material. The reaction system was then degassed for 30 min and irradiated using a 300 W xenon lamp equipped with a 400 nm cutoff filter. The photocatalytic reaction was conducted under a constant-temperature circulating water bath (10 ± 0.5°C). The amount of H_2 generated during the reaction was monitored using a gas chromatograph (GC-7920, TCD detector, high-purity N_2 as carrier gas).

Hydrogen volume was quantified via the gas chromatography system, and the amount of evolved hydrogen was calculated based on a calibration curve (Figure S1) to determine hydrogen production yield and rate.

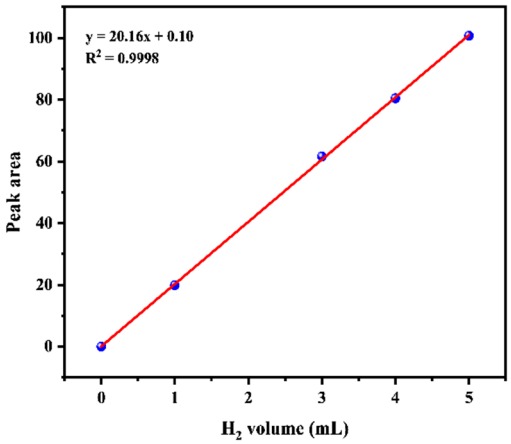

Figure S1. H_2 calibration curve

Under identical illumination conditions to those employed in the hydrogen evolution experiments, the apparent quantum efficiency (AQE) of hydrogen evolution for each catalyst was investigated[1].

$$AQY(\%) = \frac{2 \times Number\ of\ evolved\ H_2\ colecules}{Number\ of\ incident\ photons} \times 100\%$$

$$= \frac{2 \times C \times N_A}{S \times P \times t \times \frac{\lambda}{h \times c}} \times 100\%$$

Where, C is the H_2 production amount (mol) per hour; N_A is the Avogadro constant (6.02×10^{23} mol^{-1}); S is the irradiation area (cm^2); P is the monochromatic light intensity ($W\cdot cm^{-2}$); t is the light irradiation time (s); λ is the wavelength of the monochromatic light (nm); h is the Plank constant (6.626×10^{-34} J·s); c is the speed of light (3×10^8 $m\cdot s^{-1}$).

3 Results and discussion

3.1 Elemental and Structural Analysis

Table S1. The elemental percentages in Cs/PTCN-3 were determined via Energy Dispersive X-ray Spectroscopy.

Elemental	C	N	P	Cs
Atom%	64.18	33.91	0.03	1.88

*Note: The measured P content of 0.03% is close to the detection limit of the instrument, and may fall within the range of instrumental error.

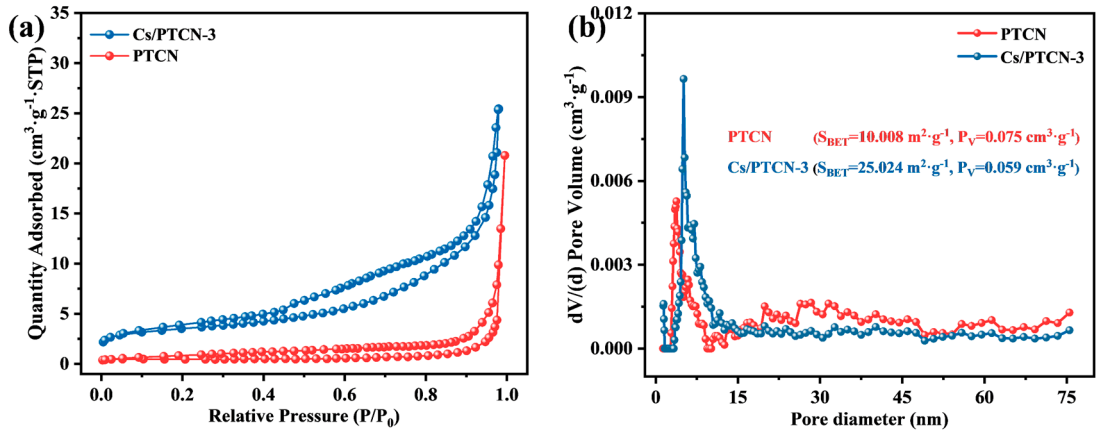

Figure S2 (a) BJH pore size distribution from the adsorption branch; (b) surface area of PTCN and Cs/PTCN-3

3.2 Evaluation of Photocatalytic Hydrogen Evolution Performance

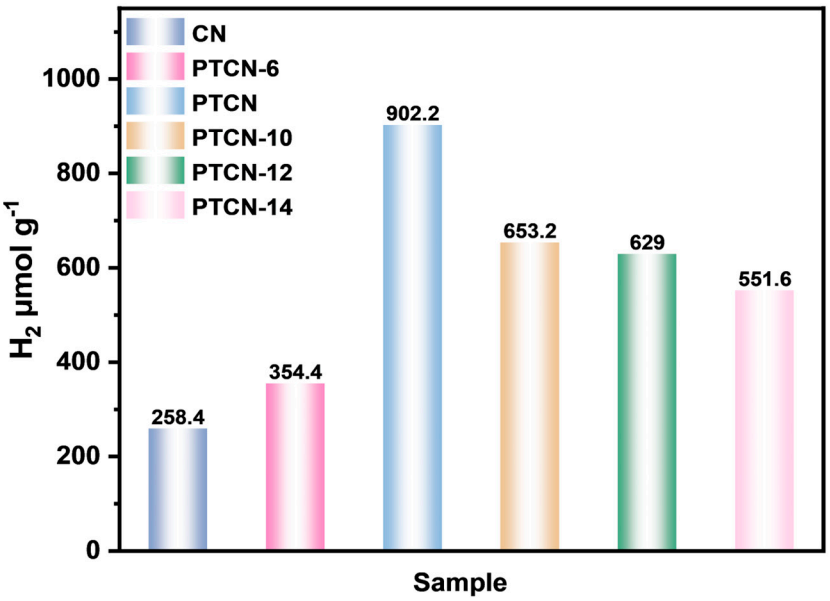

Figure S3 Hydrogen production performance of photocatalysts doped with different P concentrations through photolysis of water.

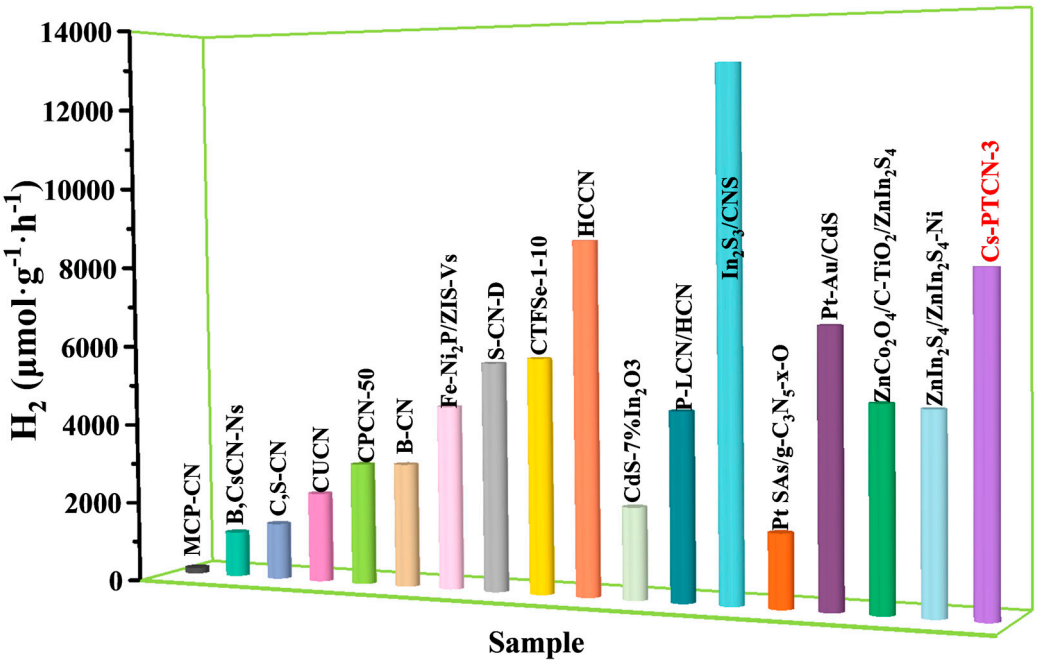

Figure S4 Comparison of hydrogen evolution performance via photocatalytic water splitting with other catalytic systems reported in the literature[2-17].

References

(1) Li, Z. Y.; Chen, Y. G.; Zhang, Y. H.; et al. Tuning interfacial charge transfer for efficient visible-light-driven photodegradation and simultaneous H_2 evolution. *Journal of Materials Science & Technology* **2024**, *168*, 35-49. DOI: 10.1016/j.jmst.2023.05.033.

(2) Tahereh, M. S.; Hossein, F.; Byeong Kyu, L.; et al. Caesium sites coordinated in Boron-doped porous and wrinkled graphitic carbon nitride nanosheets for efficient charge carrier separation and Transfer: Photocatalytic H_2 and H_2O_2 production. *Chemical Engineering Journal* **2021**, *423*, 130067. DOI: 10.1016/j.cej.2021.130067.

(3) Jang, D.; Lee, S.; Kwon, N. H.; et al. Preparation of carbon nitride nanotubes with P-doping and their photocatalytic properties for hydrogen evolution. *Carbon* **2023**, *208*, 290-302. DOI: 10.1016/j.carbon.2023.03.038.

(4) Li, G. Q.; Liang, H. O.; Fan, X. Y.; et al. Modulating and optimizing 2D/2D Fe-Ni_2P/$ZnIn_2S_4$ with S vacancy through surface engineering for efficient photocatalytic H_2 evolution. *Journal of Materials Chemistry A* **2023**, *11* (27), 14809-14818. DOI: 10.1039/d3ta02519e.

(5) Zhang, H. H.; Liu, Z.; Fang, J. Z.; et al. Modulation of π-Electron Density in Ultrathin 2D Layers of Graphite Carbon Nitride for Efficient Photocatalytic Hydrogen Production. *Small* **2024**, *20* (47), 2404929. DOI: 10.1002/smll.202404929.

(6) Dai, W.; Wang, R. H.; Chen, Z. J.; et al. Highly-efficient photocatalytic hydrogen evolution triggered by spatial confinement effects over co-crystal templated boron-doped carbon nitride hollow nanotubes. *Journal of Materials Chemistry A* **2023**, *11* (14), 7584-7595. DOI: 10.1039/d3ta00199g.

(7) Zhao, S.; Liu, Y. P.; Wang, Y. Y.; et al. Carbon and Phosphorus Co-doped Carbon Nitride Hollow Tube for Improved Photocatalytic Hydrogen Evolution. *Journal of Colloid and Interface Science* **2022**, *616*, 152-162. DOI: 10.1016/j.jcis.2022.02.057.

(8) Chen, M. H.; Xiong, J.; Li, X. Y.; et al. In-situ doping strategy for improving the photocatalytic hydrogen evolution performance of covalent triazine frameworks. *Science China Chemistry* **2023**, *66* (8), 2363-2370. DOI: 10.1007/s11426-023-1624-7.

(9) Wang, H. T.; Jiang, J. Z.; Yu, L. L.; et al. Tailoring Advanced N-Defective and S-Doped g-C_3N_4 for Photocatalytic H_2 Evolution. *Small* **2023**, *19* (28), 2301116. DOI: 10.1002/smll.202301116.

(10) Pang, Y. Y.; Li, L. J.; Bu, Q. J.; et al. Stimulating Protonation Capability by Eliminating Detrimental Defects in Crystalline Carbon Nitride for Photocatalytic Hydrogen Evolution. *Advanced Functional Materials* **2025**, 2501108. DOI: 10.1002/adfm.202501108.

(11) Wu, Y. H.; Yan, Y. Q.; Deng, Y. X.; et al. Rational construction of S-scheme CdS quantum dots/In_2O_3 hollow nanotubes heterojunction for enhanced photocatalytic H_2 evolution. *Chinese Journal of Catalysis* **2025**, *70*, 333-340. DOI: 10.1016/s1872-2067(24)60213-5.

(12) Wang, X. H.; Xue, S.; Shi, T. Y.; et al. Localized Phosphorization Manipulating Internal Electric Field Orientation in Carbon Nitride Homojunction for Efficient Photocatalytic Hydrogen Evolution. *Advanced Functional Materials* **2025**, 2424853 DOI: 10.1002/adfm.202424853.

(13) Xing, W. N.; Shao, W. F.; Li, Y. F.; et al. Rapid Charge Transfer Endowed by Heteroatom Doped Z-Scheme Van Der Waals Heterojunction for Boosting Photocatalytic Hydrogen Evolution. *Small* **2025**, *21* (10), 2412036. DOI: 10.1002/smll.202412036.

(14) Zhang, D. L.; Zhang, C.; Zhao, G. F.; et al. Single-atom Pt supported on defective graphitic carbon nitride for efficient photocatalytic hydrogen production. *Chemical Engineering Journal* **2025**, *505*, 159567. DOI: 10.1016/j.cej.2025.159567.

(15) Fan, Z. Y.; Xu, Q. H.; Wang, Y. Q.; et al. Electron regulation accelerates photocatalytic hydrogen evolution for bimetallic Pt, Au on CdS nanorods. *Chemical Engineering Journal* **2025**, *511*, 162016. DOI: 10.1016/j.cej.2025.162016.

(16) Zhang, C.; Hu, S.; Cui, W. G.; et al. Integrating photocatalytic hydrogen evolution with antibiotic degradation over a dual Z-scheme heterojunction. *Chemical Engineering Journal* **2025**, *510*, 160317. DOI: 10.1016/j.cej.2025.160317.

(17) Wang, W. B.; Liu, J.; Cui, M. X.; et al. Z-type $ZnIn_2S_4$ homojunction for high performance photocatalytic hydrogen evolution. *Chemical Engineering Journal* **2025**, *507*, 160370. DOI: 10.1016/j.cej.2025.160370.